HARDWARE AND INSTRUMENTATION – Notes

Magnetic Resonance in Medicine 72:584–590 (2014)

An Improved Trap Design for Decoupling Multinuclear RF Coils

Martin Meyerspeer,[1,2,3]* Eulalia Serés Roig,[1,4] Rolf Gruetter,[1,4,5] and Arthur W. Magill[1,4]

Purpose: Multinuclear magnetic resonance spectroscopy and imaging require a radiofrequency probe capable of transmitting and receiving at the proton and non-proton frequencies. To minimize coupling between probe elements tuned to different frequencies, LC (inductor-capacitor) traps blocking current at the ^{1}H frequency can be inserted in non-proton elements. This work compares LC traps with LCC traps, a modified design incorporating an additional capacitor, enabling control of the trap reactance at the low frequency while maintaining ^{1}H blocking.

Methods: Losses introduced by both types of trap were analysed using circuit models. Radiofrequency coils incorporating a series of LC and LCC traps were then built and evaluated at the bench. LCC trap performance was then confirmed using ^{1}H and ^{13}C measurements in a 7T human scanner.

Results: LC and LCC traps both effectively block interaction between non-proton and proton coils at the proton frequency. LCC traps were found to introduce a sensitivity reduction of 5±2%, which was less than half of that caused by LC traps.

Conclusion: Sensitivity of non-proton coils is critical. The improved trap design, incorporating one extra capacitor, significantly reduces losses introduced by the trap in the non-proton coil. **Magn Reson Med 72:584–590, 2014. © 2013 Wiley Periodicals, Inc.**

Key words: X-nucleus; RF coils; ^{13}C; trap; dual-resonant

INTRODUCTION

Multinuclear magnetic resonance imaging and spectroscopy using, for example, carbon-13 (1–3), phosphorus-31 (4–6), or sodium-23 (7–9) nuclei can provide biomedically relevant information beyond the possibilities of ^{1}H MR. Radiofrequency coils for X-nucleus detection typically include a proton channel for B_0 shimming and acquisition of scout images. Additionally, polarization of the X (low-gamma) nuclei may be enhanced via the Nuclear Overhauser Effect or polarization transfer (10), both requiring simultaneous transmission at the proton and X frequencies. Finally, the received signal may be enhanced using proton decoupling, for which the system must transmit radiofrequency energy on the proton channel while receiving on the X channel.

It is well known that probe elements tuned to the same frequency couple when brought into close proximity (11). Similarly, elements tuned to different frequencies also interact (12). The higher frequency element has relatively little influence on the resonance of the lower frequency element. However, at the higher frequency, significant current is induced in the lower frequency element, affecting both the resonant frequency and field profile of the higher frequency element. Therefore, in a multinuclear probe it is important to suppress interactions between the X and ^{1}H channels at the ^{1}H frequency.

One approach to prevent coupling at the higher frequency is to insert traps into the X nucleus coil(s) (13–15) tuned to selectively block current induced at the proton frequency while allowing the coil to resonate at the lower X frequency. Adding extra components to the low frequency coils slightly degrades the coils' sensitivity. However, in contrast to geometric decoupling (16–18), trapped coils impose no constraints on the relative positions of the proton and X nucleus coil elements.

This work compares *LC* traps, consisting of a parallel inductor and capacitor, with *LCC* traps, introduced by Webb et al. (19), which include a second capacitor in the trap circuit. Both traps block current at the ^{1}H frequency, but while *LC* traps present a small inductive reactance at the X nucleus frequency, the extra capacitor in *LCC* traps allow control over the trap reactance at the X frequency. *LCC* traps may thus be designed to replace a coil capacitor, reproducing its reactance at the low frequency while simultaneously presenting a high impedance at the high frequency. Here, we compare the impact of *LCC* traps on radiofrequency coil sensitivity with that of *LC* traps, using circuit modeling and bench measurements. The effectiveness of *LCC* traps in ^{1}H and ^{13}C NMR measurements is then shown using a 7 T human scanner.

METHODS

LCC traps may be designed to block current at the ^{1}H frequency while reproducing the reactance of a chosen coil

[1]LIFMET, École Polytechnique Fédérale de Lausanne, Lausanne, Switzerland.

[2]Center for Medical Physics and Biomedical Engineering, Medical University of Vienna, Austria.

[3]MR Centre of Excellence, Medical University of Vienna, Austria.

[4]Department of Radiology, University of Lausanne, Lausanne, Switzerland.

[5]Department of Radiology, University of Geneva, Geneva, Switzerland.

Grant sponsor: Austrian Science Fund FWF; Grant number: J3013-N20 (to M.M.); Grant sponsors: Centre d'Imagerie Biomédicale (CIBM) of the Université de Lausanne; Université de Genève; Hôpitaux Universitaires de Genève; Centre Hospitalier Universitaire Vaudois and Ecole Polytechnique Fédérale de Lausanne; Leenaards and Jeanet Foundations.

*Correspondence to: Martin Meyerspeer; Center for Medical Physics and Biomedical Engineering, Medical University of Vienna, Austria.
E-mail: martin.meyerspeer@meduniwien.ac.at.

Received 1 July 2013; revised 1 July 2013; accepted 30 July 2013
DOI 10.1002/mrm.24931
Published online 4 September 2013 in Wiley Online Library (wileyonlinelibrary.com).

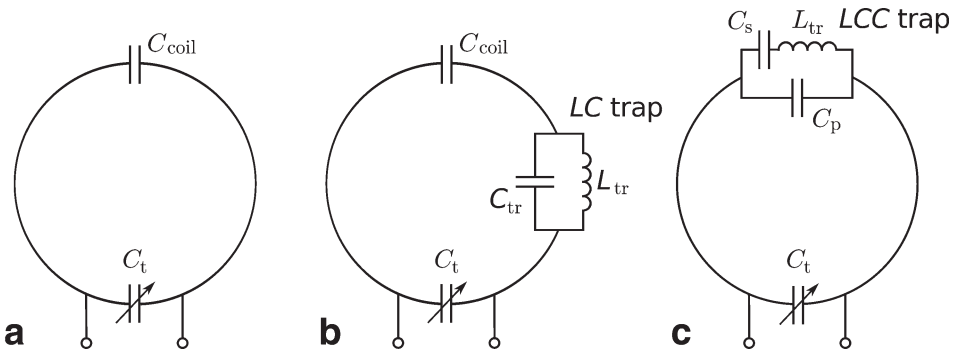

FIG. 1. Circuit schematics for (**a**) an untrapped loop, (**b**) a loop coil including an *LC* trap, and (**c**) the modified circuit bringing the series capacitance into the trap, forming an *LCC* trap.

capacitor at the X-nucleus frequency. The conditions for the trap reactance X_{tr} at the two frequencies are

$$X_{tr} = \mathrm{im}\,(Z_{tr}) = \begin{cases} X_{C_{coil}} = -\dfrac{1}{\omega C_{coil}} & \text{at } \omega = \omega_L \\ 0 & \text{at } \omega = \omega_H \end{cases}, \quad [1]$$

where ω_L and ω_H indicate the Larmor frequencies of the X and ^{1}H nuclei, respectively. Solving the analytical expression of the *LCC* trap's (Fig. 1c) reactance X_{tr} for the trap capacitors C_s and C_p under the conditions given in Eq. 1 yields a pair of solutions:

$$C_s = \frac{\left(\omega_H^2 + \omega_L^2\right)}{(\omega_L\omega_H)^2 L_{tr} + \dfrac{\left(\omega_H^2 - \omega_L^2\right)}{C_{coil}}} \times \left(\frac{1}{2} \pm \sqrt{\frac{1}{4} - \frac{(\omega_L\omega_H)^2 L_{tr} + \dfrac{\left(\omega_H^2 - \omega_L^2\right)}{C_{coil}}}{L_{tr}\left(\omega_H^2 + \omega_L^2\right)^2}} \right)$$

$$C_p = \left(\omega_H^2 L_{tr} - \frac{1}{C_s}\right)^{-1} \quad [2]$$

Valid solutions for C_s and C_p imply that the radicand in Eq. 2 is positive, hence a minimum trap inductance

$$\min\,(L_{tr}) = \frac{1}{C_{coil}} \frac{4}{\omega_H^2 - \omega_L^2} \quad [3]$$

exists for given resonance frequencies and coil capacitor to be replaced by the *LCC* trap.

Modeling Sensitivity

To estimate the effect of an *LCC* trap on the X coil efficiency, additional resistance introduced into the coil by the trap was modeled. In analogy to the model described by Dabirzadeh et al. (15) the relative signal-to-noise ratio (SNR) of a trapped versus an untrapped coil is

$$\frac{\mathrm{SNR}_{\,\mathrm{trapped}}}{\mathrm{SNR}_{\,\mathrm{untrapped}}} = \sqrt{\frac{R_{coil}}{R_{coil} + R_{tr}}}, \quad [4]$$

where $R_{coil} = \omega_L L_{coil}/Q_{coil}$. We assume a loaded quality factor $Q_{coil} = 65$, which is realistic for in vivo conditions. The traps' equivalent series resistance R_{tr} was modeled as the loss due to resistance of the trap inductor $R_{L_{tr}} = \omega_L L_{tr}/Q_{tr}$. For an *LC* trap the analytical expression for R_{tr} expands to

$$R_{tr} \approx R_{L_{tr}}/\left(1 - \omega_L^2/\omega_H^2\right)^2, \quad [5]$$

which shows that the resistance of an *LC* trap is always larger than the resistance of its inductor, for example, $R_{tr} \approx 1.14 R_{L_{tr}}$ for a trap blocking ^{1}H in a ^{13}C coil.

For *LCC* traps, the ratio of R_{tr} to $R_{L_{tr}}$ depends on how close the resonant frequency of the series branch $\omega_s = 1/\sqrt{L_{tr} C_s}$ is to the trap blocking frequency

$$R_{tr} \approx R_{L_{tr}} \left(\frac{\omega_H^2 - \omega_s^2}{\omega_H^2 - \omega_L^2}\right)^2, \quad [6]$$

which is always smaller than $R_{L_{tr}}$ for $\omega_L < \omega_s < \omega_H$ (e.g., $R_{tr} \approx 0.82\, R_{L_{tr}}$ for $L_{tr} = 40$ nH).

The trap resistances $R_{tr}(L_{tr})$ were also simulated numerically for both types of traps, including the resistive losses of solder joints [$r_s = 25\mathrm{m}\Omega$ (20)] connecting the trap components in the model. Numeric solutions were identical to the analytic results when the solder joint resistance was set to zero.

An inductor's equivalent series resistance $R_{L_{tr}}$ generally depends on L_{tr} and frequency. To estimate $R_{L_{tr}}(L_{tr})$ at ω_L, the frequency at which the trap passes current, the quality factor Q_{tr} of the traps in isolation was measured using a pair of sniffer loops overlapped for mutual flux cancellation (21), connected to a network analyzer (E5071C Agilent Technologies, Santa Clara, CA, USA). Trap capacitors were exchanged to resonate the trap at ω_L rather than ω_H, while preserving the traps' geometric arrangement. Resistances $R_{L_{tr}}$ were then calculated from measured Q_{tr} values, assuming the choke and solder joints being the only lossy elements. $R_{L_{tr}}(L_{tr})$ was parameterized using linear regression (the coefficient of determination was $R^2 = 0.99$ for both types of traps), to express trapped coil SNR as functions of L_{tr}.

Coil Construction and Bench Measurements

A pair of coplanar concentric loop coils was built from copper wire (3 mm diameter), non-magnetic ceramic chip capacitors (100E, American Technical Ceramics Corp., NY, USA) and variable capacitors for matching and tuning (Sprague-Goodman, NY, USA). The outer loop (11 cm diameter, four loop capacitors and no trap)

Table 1
Unloaded and Loaded Quality Factors (Q_U, Q_L) of Trapped and Untrapped ^{13}C coils, with and without ^{1}H Coil Present

	^{13}C coil, ^{1}H coil absent			*^{13}C coil, ^{1}H coil present*		
RF bench	Q_U	Q_L	Q_U/Q_L	Q_U	Q_L	Q_U/Q_L
Untrapped	278	71	3.9	268	70	3.8
LC trap	137	67	2.0	137	65	2.1
LCC trap	215	75	2.9	212	72	2.9

The trap inductance was $L_{tr} = 40$ nH.

was tuned to 297 MHz for ^{1}H at 7 T. The inner loop (6 cm diameter, 120 nH inductance, two capacitors on the loop) was tuned to 74.7 MHz for ^{13}C.

Three versions of the inner loop were built: (a) untrapped, $C_{coil} = 78$ pF; (b) with $C_{coil} = 78$ pF and an *LC* trap; and (c) replacing C_{coil} with an *LCC* trap (Fig. 1). For the trapped coils, traps were built using inductors in the range 16–95 nH. Chokes were wound from copper wire ($d = 1$ mm) using four turns at different diameters, to maintain comparable geometry. Each trap was assembled and its resonance frequency and *Q*-factor were measured in isolation, using a pair of overlapped sniffer loops connected to a network analyzer.

Bench measurements were performed with the ^{1}H coil alone, with the untrapped ^{13}C coil (Fig. 1a), and with the different *LC* and *LCC* traps (Fig. 1b,c). Where values are given under loaded conditions, in vivo loading was mimicked using a saline bottle placed below the coils. To measure sensitivity, transmission between the coil and a single sniffer loop was determined along the axis of the concentric coils. Reported amplitudes represent the average ± standard deviation over four measurements acquired at the coil centres.

NMR measurements

An untrapped coil and an otherwise identical *LCC* trapped coil ($L_{tr} = 40$ nH, $C_s = 47$ pF, $C_p = 8.2$ pF) were compared while positioned concentrically inside a ^{1}H coil, in a 7 T human scanner (Magnetom, Siemens Healthcare Sector, Erlangen, Germany).

To show the effect of the trap on ^{1}H performance, gradient echo images ($T_E = 1.4$ ms, $T_R = 10$ ms, matrix size: 192×150, field of view: 198×154 mm^2, 52 slices, 3.8 mm slice thickness) were acquired with the ^{1}H coil alone and in the presence of an untrapped and a trapped ^{13}C coil. The phantom was a 4 L bottle, filled with saline solution approximately matching the load of a human head.

To test the effect of the *LCC* trap on ^{13}C sensitivity, spectra were acquired from an 8 mm sphere filled with formic acid (3.5% concentrations, 100% ^{13}C enrichment, Gd doped), which was centered in the 6 cm coil. To compare the transmit efficiencies of the two coils, the formic acid resonance was excited using a 0.5 ms block pulse and fully relaxed free induction decay spectra were acquired without averaging (2048 spectral points, 8 kHz spectral width). The transmit voltage U_{TX} was increased from 10 to 230 V in 10 V steps, and a sine

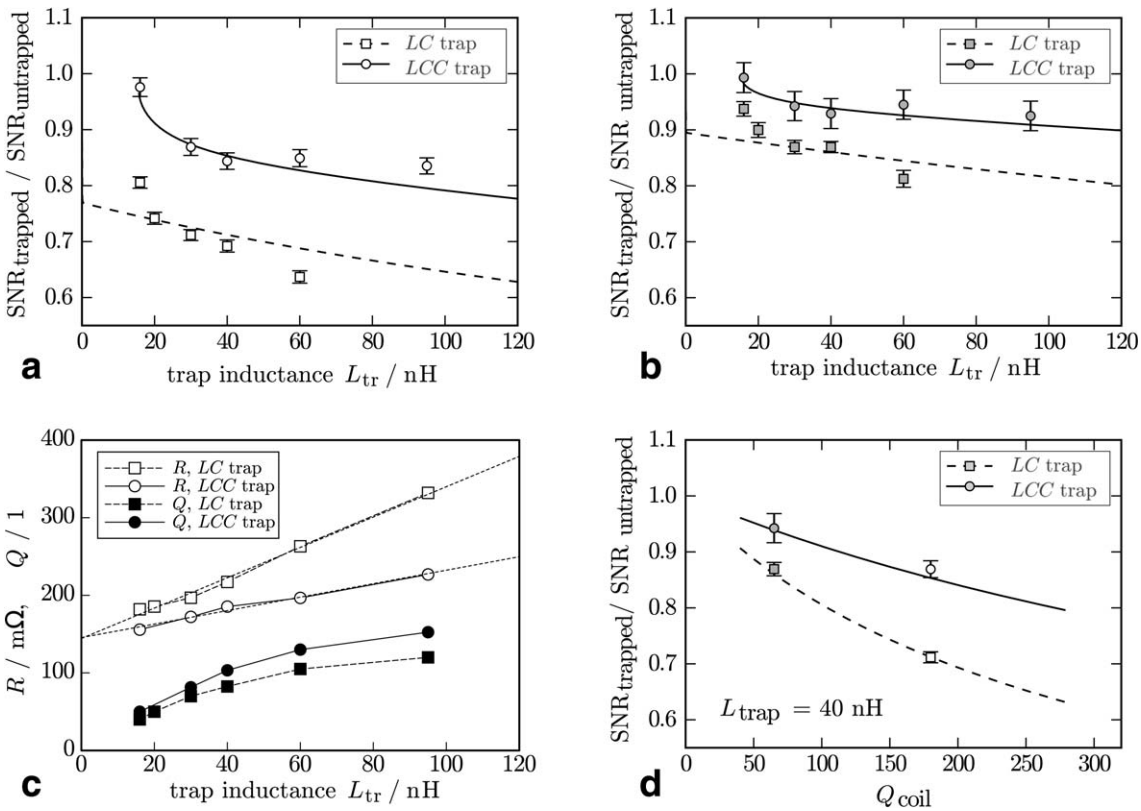

FIG. 2. Sensitivity of trapped ^{13}C coils, measured and simulated (lines), relative to an untrapped coil under (**a**) unloaded ($Q_{coil} = 185$) and (**b**) loaded ($Q_{coil} = 65$) conditions (measurements were performed using a single sniffer loop and repeated four times); (**c**) measured *Q*-factors, and hence resistance, of the trap inductors at ω_L; and (**d**) the dependence of coil sensitivity on loading.

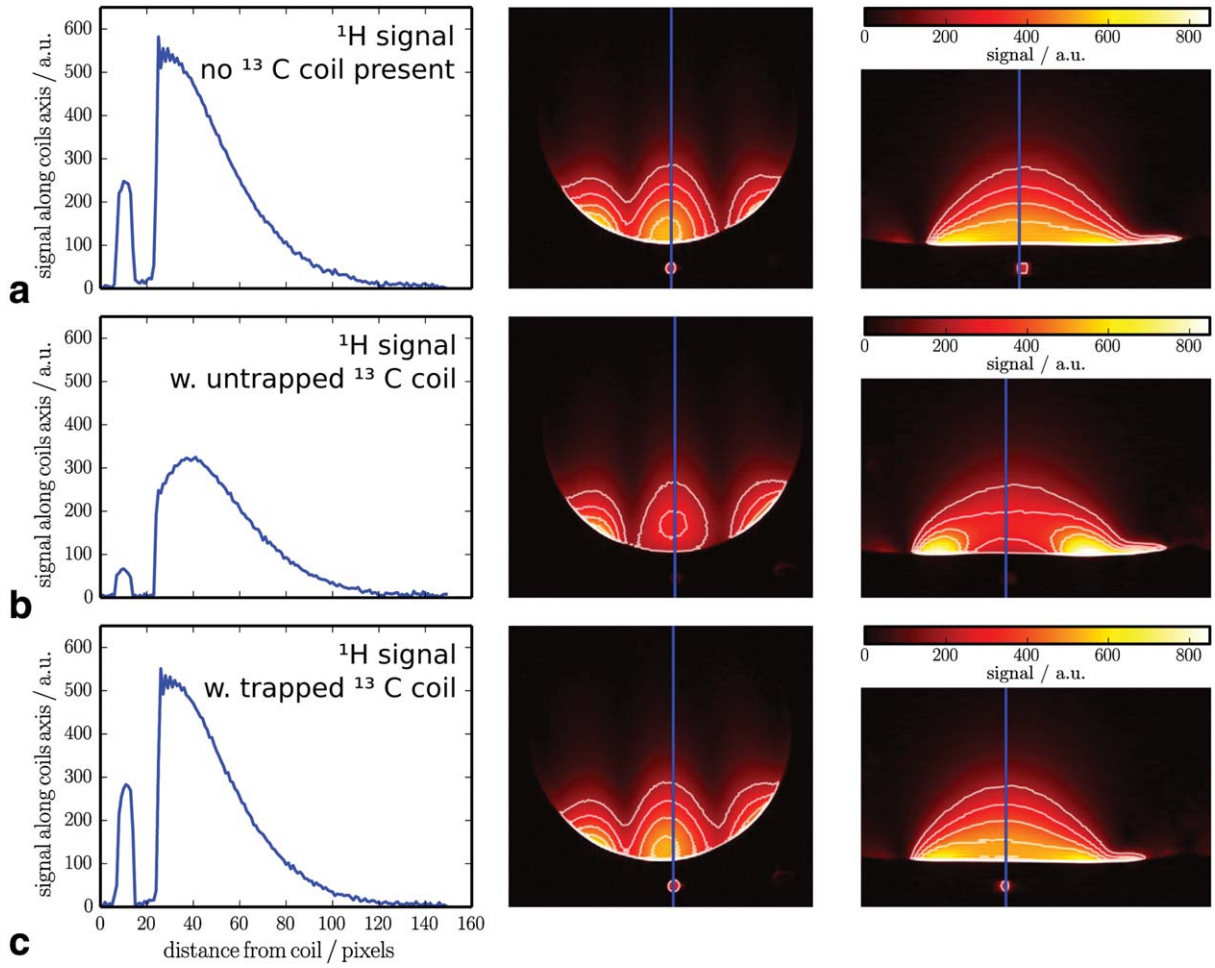

FIG. 3. Gradient echo images and image intensity profiles along the coil's symmetry axis of an 11 cm ^{1}H loop coil (**a**). Strong signal cancellation occurs when an untrapped 6 cm ^{13}C coil is placed concentrically in the plane of the ^{1}H coil (**b**). The signal loss is completely recovered by including an *LCC* trap in the ^{13}C coil (**c**). Contours mark image intensities from 200 to 500 a.u., in steps of 100.

function of U_{TX} was fitted to the resulting signal. The ^{13}C SNR was compared between the untrapped and the trapped coil using eight fully relaxed free induction decay spectra, acquired following excitation with an adiabatic half passage pulse (smoothed chirp pulse, duration = 1 ms, U_{TX} = 70 V).

To verify that ^{1}H decoupling of ^{13}C spectra was possible while using a trapped coil, spectra were measured using a two-compartment phantom (a 120 mL compartment filled with glycogen, 800 mmol/L, inside a 2 L bottle containing ^{13}C C1-labeled glucose, 8 mmol/L). Free induction decay (8 kHz spectral width, 2048 points, 512 averages) were acquired without and with heteronuclear continuous wave decoupling. The decoupling ^{1}H pulse frequency was set to the resonance of the coupling partner of glycogen. Decoupling was applied at 90 V for the full acquisition time. Noise was quantified as standard deviation of the spectra (without apodization or zero filling) in four consecutive regions of 500 Hz width, starting 1 kHz upfield from the glycogen resonance.

Magnetic resonance spectroscopy data for the B_1 transmit efficiency measurements were fitted in the time domain using the AMARES (22) routine from jMRUI (23). SNR was quantified as peak amplitude divided by

Table 2
Transmit Efficiency (γ/B_1 at U_{TX} = 100 V in the coil centre) and SNR of Spectra of Formic Acid, Acquired with a 6 cm ^{13}C Loop Coil With and Without an *LCC* trap

^{13}C MRS	γ/B_1 (Hz) Mean±SD	SNR FA peak 1	SNR FA peak 2	LW (Hz) Mean±SD	SNR · LW (Hz) Mean±SE
Untrapped	1580±3	133±9	131±9	20.9±0.4	5130±90
Trapped	1563±3	129±7	126±6	20.2±0.4	4870±70
Difference	−1.1±0.2%				−5.0±2.2%

For the comparison, SNR was multiplied by line width (LW).

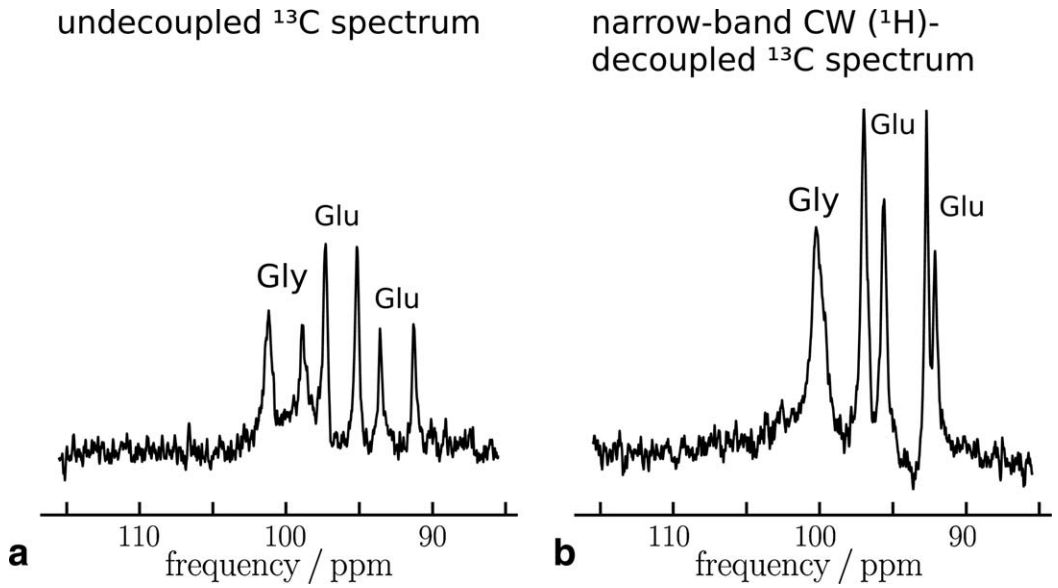

FIG. 4. ^{13}C NMR spectra of a phantom containing glycogen and glucose (**a**) undecouped and (**b**) with narrow-band continuous wave decoupling of the glycogen resonance, demonstrating that the trapped ^{13}C coil can withstand decoupling power without inducing additional artifacts or noise.

standard deviation of data points from an artefact-free flat baseline region of the spectra after zero filling and Lorentzian apodization (matched filter, line width ~20 Hz). SNR quantification and all other data processing and simulations in this work were done using programs written in Python. All measurement results are given as mean ± standard deviation, except where indicated otherwise.

RESULTS

Bench Measurements

To evaluate the effect of *LC* and *LCC* traps on coil sensitivity, B_1 field and *Q* measurements were performed on the bench. Bringing the ^{1}H coil close to the ^{13}C coils caused no frequency shift. The *Q*-factors of the ^{13}C coils reduced by 3±5% when unloaded, and 2±2% when loaded, averaged over all coils (untrapped, and *LC* and *LCC* trapped with $L_{tr} = 16$–95 nH). The average loaded to unloaded quality factor ratio Q_U/Q_L was higher for coils with *LCC* traps (3.2±0.4) than for coils with *LC* traps (2.2±0.3), while for the untrapped coil it was 3.9. Unloaded and loaded *Q*-factors for exemplary traps with $L_{tr} = 40$ nH, the inductance used in NMR experiments, are given in Table 1.

Proton traps caused a decrease in ^{13}C coil sensitivity, which was more pronounced with increasing trap inductance L_{tr}. Measurements performed with the unloaded (Fig. 2a) and loaded (Fig. 2b) coils showed that *LCC* traps (circles) always outperform *LC* traps (squares) using the same inductance. In most cases, *LCC* traps also outperformed *LC* traps with smaller inductors. For both trap designs, using a larger inductor provided better blocking at the ^{1}H frequency.

A pairwise comparison of *LC* and *LCC* traps, with $L_{tr} = 30$, 40, and 60 nH, showed that the sensitivity loss due to *LCC* traps was only 46±5% of the loss caused by *LC* traps with the coil unloaded, and 43±13% with the coil loaded. These findings were confirmed using circuit model simulations. Trap inductor resistances were measured by retuning traps to ω_L and measuring their *Q*-factors (Fig. 2c). These values were then inserted into the circuit model. Simulated sensitivities of ^{13}C coils with *LC* and *LCC* traps closely matched sensitivities measured experimentally using a sniffer loop (Fig. 2a,b). The sensitivity drop was more pronounced for unloaded (Fig. 2a) than for loaded coils (Fig. 2b), which is also evident in Fig. 2d, showing the simulated sensitivity as function of coil load (decreasing Q_{coil}) with experimentally established data points at two different coil loads.

Placing the untrapped ^{13}C coil concentrically inside the ^{1}H coil caused its resonance frequency to shift from 297 to 305 MHz, strongly impairing its sensitivity and requiring retuning. In the coil plane, the B_1 amplitude was reduced by 67±1% when unloaded, and by 63±0.2% when loaded. When trapped ^{13}C coils were placed inside the ^{1}H coil, no shift of the ^{1}H coil's resonant frequency was observed. Reductions in B_1 were 20±3% for unloaded coils dropping by 25% with *LC* traps and by 19% with *LCC* traps, while ^{1}H coil sensitivity was fully restored to 107±5% in the loaded case (averaged over all traps with $L_{tr} = 30$, 40, and 60 nH).

A larger inductor L_{tr} provided better isolation between the coil elements at the ^{1}H frequency, particularly for *LC* traps, which showed −45 to −55 dB isolation, depending on L_{tr}. *LCC* traps provided better than −60 dB of isolation in all cases, except for the trap with the smallest theoretically feasible inductor ($L_{tr} = 16$ nH), which provided −40 dB of isolation and incurred a sensitivity reduction of 54% when unloaded.

NMR Measurements

The effect of untrapped and trapped ^{13}C coils on ^{1}H coil performance was demonstrated using gradient-echo

images. Figure 3a was acquired with the ^{1}H coil only. When the untrapped ^{13}C coil was placed inside the ^{1}H coil, strong signal cancellation was observed (Fig. 3b), decreasing the signal amplitude by 52±5% near the coil plane, measured over $10 \times 10 \times 5$ voxels. With the trapped ^{13}C coil, the signal was recovered to 100±5% (Fig. 3c).

In ^{13}C spectroscopy measurements with the untrapped and trapped ^{13}C coils, maximum signal from the coil centre was reached at $U_{TX} = 32.5$ V using a 0.5 ms block pulse. The B_1 field at the coil centre was calculated by fitting a sine function to the peak signal amplitude in a series of measurements at a range of transmit voltages; it was found to differ only by −1.1±0.2% for the two coils at a reference voltage of $U_{TX} = 100$ V (Table 2). Consistent with the small decrease of B_1 transmit performance, the SNR measured repeatedly in pulse-acquire spectra after adiabatic excitation was decreased by only 5.0±2.2% (mean±SE) using the trapped coil, compared to an untrapped ^{13}C coil.

Continuous-wave ^{1}H decoupling did not induce additional noise; that is, no significant difference of the noise level was found in the spectra, with 100±5 a.u. in the undecoupled spectra, versus 96±7 a.u. in decoupled spectra, which show the glycogen resonance to be fully decoupled (Fig. 4, with 5 Hz Lorentzian apodisation and zero filling to 16 k points, for display).

DISCUSSION AND CONCLUSIONS

This work compares *LC* traps, consisting of a parallel inductor and capacitor, with *LCC* traps that include an additional capacitor in series with the inductor. Traps were built into a ^{13}C coil to suppress interaction between it and a ^{1}H coil, while minimizing loss in the ^{13}C coil.

LCC traps allow control over the trap's blocking frequency, and reactance at the X-nucleus resonance frequency. Bench measurements with a series of trap inductors demonstrated that the sensitivity decrease of non-proton coils caused by *LCC* traps was less than half that introduced by *LC* traps. This benefit can be substantial, particularly for weakly loaded coils, for example, 10% vs. 30% loss when $Q = 180$ (see Fig. 2).

The higher sensitivity of coils with *LCC* traps, compared to *LC* traps, can be explained by modeling the resistive losses in each trap circuit. The resistance of an *LC* trap is always larger than the series resistance of the trap inductor (Eq. 5) and, when the choke's resistive losses dominate, depends only on the ratio of the Larmor frequencies of the nuclei. In contrast, an *LCC* trap's resistance is always smaller than the resistance of the trap inductor (Eq. 6), and depends on the inductance value, explicitly and implicitly via C_s and C_p. The resistance of the inductors used was measured via the quality factor of the isolated traps, retuned to resonate at the X nucleus Larmor frequency, and included in the model of the trapped coils' sensitivities.

For both types of trap, a higher trap inductance L_{tr} causes more efficient blocking at the ^{1}H frequency but incurs higher losses at the X nucleus frequency. In contrast to *LC* traps, the inductor used for a *LCC* trap must be chosen above a minimum value that depends on C_{coil}, ω_H, and ω_L, as determined by Eq. 3. Nevertheless, even when using larger L_{tr}, the sensitivity of the ^{13}C coil with *LCC* traps was superior compared to coils with *LC* traps. Traps tested on the bench used inductors ranging from the minimum feasible value of 16 nH, to 95 nH, in a 120 nH loop coil. The trap inductance chosen for MR measurements was $L_{tr} = 40$ nH, which resulted in excellent blocking and a very low sensitivity reduction.

We note that the circuit of a coil including a trap for proton blocking is identical to that of a dual-resonant coil (24). Dual-resonant coils built using *LCC* traps should, therefore, provide a similar sensitivity enhancement at the low frequency, in comparison to traditional designs using *LC* traps.

We conclude that *LCC* proton traps can effectively block current induced in an X nucleus coil at the ^{1}H frequency, while incurring only a very small reduction of coil sensitivity (5±2%), which was found to be less than half that possible with comparable *LC* traps. We further conclude that *LCC* traps can be used in place of a capacitor in an existing coil design, allowing well-established designs to be applied to multinuclear coils.

REFERENCES

1. Chance B, Eleff S, Leigh JS. Noninvasive, nondestructive approaches to cell bioenergetics. Proc Natl Acad Sci USA 1980;77:7430–7434.
2. Rothman DL, Magnusson I, Katz LD, Shulman RG, Shulman GI. Quantitation of hepatic glycogenolysis and gluconeogenesis in fasting humans with ^{13}C NMR. Science 1991;254:573–576.
3. Gruetter R, Adriany G, Choi IY, Henry PG, Lei H, Oz G. Localized in vivo ^{13}C NMR spectroscopy of the brain. NMR Biomed 2003;16:313–338.
4. Chance B, Leigh JS, Kent J, McCully K, Nioka S, Clark BJ, Maris JM, Graham T. Multiple controls of oxidative metabolism in living tissues as studied by phosphorus magnetic resonance. Proc Natl Acad Sci USA 1986;83:9458–9462.
5. Kemp GJ, Radda GK. Quantitative interpretation of bioenergetic data from ^{31}P and ^{1}H magnetic resonance spectroscopic studies of skeletal muscle: an analytical review. Magn Reson Q 1994;10:43–63.
6. Meyerspeer M, Robinson S, Nabuurs CI, Scheenen T, Schoisengeier A, Unger E, Kemp G, Moser E. Comparing localized and nonlocalized dynamic ^{31}P magnetic resonance spectroscopy in exercising muscle at 7T. Magn Reson Med 2012;68:1713–1723.
7. Babsky AM, Topper S, Zhang H, Gao Y, James JR, Hekmatyar SK, Bansal N. Evaluation of extra- and intracellular apparent diffusion coefficient of sodium in rat skeletal muscle: effects of prolonged ischemia. Magn Reson Med 2008;59:485–491.
8. Hussain MS, Stobbe RW, Bhagat YA, et al. Sodium imaging intensity increases with time after human ischemic stroke. Ann Neurol 2009; 66:55–62.
9. Trattnig S, Welsch GH, Juras V, Szomolanyi P, Mayerhoefer ME, Stelzeneder D, Mamisch TC, Bieri O, Scheffler K, Zbn S. 23Na MR imaging at 7 T after knee matrix-associated autologous chondrocyte transplantation preliminary results. Radiology 2010;257:175–184.
10. de Graaf RA. In vivo NMR Spectroscopy. West Sussex: Wiley; 1998, p. 508.
11. Roemer PB, Edelstein WA, Hayes CE, Souza SP, Mueller OM. The NMR phased array. Magn Reson Med 1990;16:192–225.
12. Fitzsimmons JR, Beck BL, Brooker HR. Double resonant quadrature birdcage. Magn Reson Med 1993;30:107–114.
13. Alecci M, Romanzetti S, Kaffanke J, Celik A, Wegener HP, Shah NJ. Practical design of a 4 Tesla double-tuned RF surface coil for interleaved ^{1}H and ^{23}Na MRI of rat brain. J Magn Reson 2006;181:203–211.
14. Dabirzadeh A, Chang CW, McDougall MP. An insertable P-31 RF coil for Dual-frequency Magnetic Resonance Imaging & Spectroscopy. In Proceedings of the 30th Annual International IEEE EMBS Conference, Vancouver, BC, Canada: IEEE Eng Med Biol Soc; 2008. pp. 2036–2038.
15. Dabirzadeh A, McDougall MP. Trap design for insertable second-nuclei radiofrequency coils for magnetic resonance imaging and spectroscopy. Concepts Magn Reson B 2009;35B:121–132.

16. Bottomley PA, Hardy CJ, Roemer PB, Mueller OM. Proton-decoupled, Overhauser-enhanced, spatially localized carbon-13 spectroscopy in humans. Magn Reson Med 1989;12:348–363.
17. Adriany G, Gruetter R. A half volume coil for efficient proton decoupling in humans at 4 Tesla. J Magn Reson 1997;125:178–184.
18. Peshkovsky AS, Kennan RP, Fabry ME, Avdievich NI. Open half-volume quadrature transverse electromagnetic coil for high-field magnetic resonance imaging. Magn Reson Med 2005;53:937–943.
19. Webb A, Smith N. ^{31}P spectroscopy in human calf muscle at 7 Tesla using a balanced double-quadrature proton-phosphorus RF coil. In Proceedings of the 18th Annual Meeting ISMRM, Stockholm, Sweden, 2010. #3818.
20. Kumar A, Edelstein WA, Bottomley PA. Noise figure limits for circular loop MR coils. Magn Reson Med 2009;61:1201–1209.
21. Darrasse L, Kassab G. Quick measurement of nmrcoil sensitivity with a dualloop probe. Rev Sci Instrum 1993;64:1841.
22. Vanhamme L, van den Boogaart A, van Huffel S. Improved method for accurate and efficient quantification of MRS data with use of prior knowledge. J Magn Reson 1997;129:35–43.
23. Naressi A, Couturier C, Devos JM, Janssen M, Mangeat C, de Beer R, Graveron-Demilly D. Java-based graphical user interface for the MRUI quantitation package. Magn Reson Mater Phy 2001;12:141–152.
24. Schnall MD, Harihara Subramanian V, Leigh JS. The application of overcoupled tank circuits to NMR probe design. J Magn Reson 1986;67:129–134.